Journal of Biomedical Optics 8(2), 185–190 (April 2003)

Infrared microspectroscopic imaging maps the spatial distribution of exogenous molecules in skin

Richard Mendelsohn
Hui-Chen Chen
Rutgers University
Department of Chemistry
73 Warren Street
Newark, New Jersey 07102

Mark E. Rerek
ISP Corporation
1360 Alps Road
Wayne, New Jersey 07470

David J. Moore
Unilever Research US
45 River Road
Edgewater, New Jersey 07020
E-mail: david.j.moore@unilever.com

Abstract. Infrared (IR) microscopic imaging is used, in a series of proof-of-principle experiments to map the spatial distribution of two penetration enhancers, dimethylsulphoxide (DMSO) and propylene glycol, in skin. The current instrumentation utilizes a 64×64 array of IR detectors imaged at the focal plane of an IR microscope, each collecting a complete mid-infrared spectrum of the skin section on each pass of the interferometer. The spatial area sampled by each element in the array is ~6.3×6.3 μm. Any spectral parameter (e.g., arising from lipid or protein vibrational modes of the endogenous tissue or the exogenous component) may be quantitatively analyzed across the entire array of 4096 spectra, thereby generating an IR spectroscopic image of that particular parameter throughout the sample. The images directly reveal the spatial heterogeneity of the protein and lipid distributions. In transverse slices of skin, the depth dependencies of the spatial distribution of triglyceride and protein have been monitored, and compared to those of the exogenous penetration enhancers. Images of both DMSO and propylene glycol suggest that each penetrates the skin to a depth of at least 1 mm (under our experimental protocols), and reveals a spatial distribution that is essentially coincident with the protein constituents of the skin. These results demonstrate that IR microscopic imaging has great potential for mechanistic studies of topical, dermal, and transdermal delivery.
 [DOI: 10.1117/1.1560645]

Keywords: infrared imaging; skin; drug delivery; penetration enhancers.

Paper 02042 received Jul. 3, 2002; revised manuscript received Nov. 22, 2002; accepted for publication Nov. 25, 2002.

1 Introduction

The molecular level determination of dermal and transdermal percutaneous absorption pathways is of interest in several areas of dermatological research and drug delivery research. For example, optimal therapeutic intervention may require delivery of drugs at particular concentrations to well-defined locations within the skin. In addition, knowledge of permeation pathways of penetration-enhancing molecules would provide a quantitative basis for understanding the thermodynamic and kinetic mechanisms of action of these substances.

Various research groups have probed lipid behavior and protein secondary structures in epidermis, as well as stratum corneum (SC) models, using infrared (IR) spectroscopy techniques.[1–4] Furthermore, *in-vivo* and *ex-vivo* attenuated total reflectance (ATR) techniques have been applied to examine the outer layers of skin and thereby probe hydration, drug delivery, and percutaneous absorption.[5–7] Several biomedical studies by the Canadian National Research Council Biodiagnostics group have demonstrated the ability of infrared (both mid-IR and near-IR) spectroscopy to differentiate pathological skin samples.[8,9] However, two significant limitations of traditional IR sampling techniques are: 1. the requirement that samples be homogenized and that each spectrum is thus an average from a large sample area: or, if IR-microspectroscopy is used to avoid sample homogenization, 2. the problem of slow image accumulation in point-by-point IR microspectroscopy.

The commercial availability of mid-IR array detectors has overcome the limitation of traditional IR microscopy sampling. This has resulted in the introduction of IR imaging spectrometers and opened up a new field; mid-IR microspectroscopic imaging. Our current instrumentation consists of a 64×64 array of IR detectors imaged to the focal plane of an IR microscope. On each pass of the interferometer, a complete IR spectrum is collected from each array element, thus 4096 spectra are acquired in about the same time required to generate a single spectrum with a standard IR microscope. This approach constitutes true mid-IR spectroscopic imaging and results in a gain of about 1000 in time (to achieve equivalent signal to noise ratio) compared to point-by-point IR microscopy. Acquisition of the raw sample data (a matrix of 64 ×64 spectra) takes approximately 5 min. Initial applications of this technology to tissues have included studies of the hydroxyapatite and collagen constituents of bone,[10] silicone in breast biopsies,[11] and the distribution of lipids and proteins in slices of brain tissue.[12] In addition, recent studies by Diem et al. have revived the long-standing hope that IR microscopy will be useful in the field of cancer detection.[13]

The current study describes our initial applications of IR microspectroscopic imaging to monitor the permeation and

1083-3668/2003/$15.00 © 2003 SPIE

tissue distribution of two known dermal penetration enhancers, propylene glycol (PG) and dimethylsulphoxide (DMSO) in porcine skin, and demonstrates the potential of this technique for fields such as transdermal and dermal drug delivery.

2 Experimental Section

2.1 *Sample Preparation*

Full-thickness porcine skin was obtained from hairless pigs and cut into small sections (1.5×1.5 cm) for mounting in cryostat for cryosectioning. For transmission IR spectroscopic techniques, tissue sections are routinely required to be ~2 to 10 μm thick. Samples for the current study were prepared using a Leica 1800 cryostat and were adhered on their side to a mounting block with cryostat fixing solution. After cryofixing samples by freezing to −60 °C, sections were sliced to a thickness of either 5 or 8 μm. In general, very good samples for spectroscopy could be obtained in this orientation (i.e., sections sliced perpendicular to the skin surface), since a smooth, flat surface could be prepared by making many passes with the knife before collecting a section appropriate for IR measurements. Prior to sectioning, skin samples were treated with deuterated PG or deuterated DMSO solutions applied to the external stratum corneum surface for defined time periods. For this initial IR imaging study, concentrations and application times were taken from previously reported literature protocols.[14] Solutions of DMSO and DPG (approximately 15 μL/cm^2) were applied to the SC surface of porcine skin and left for 3 h, after which the skin surface was wiped clean to remove all remaining material.

2.2 *Fourier Transform Infrared Microscopic Imaging*

Spectra were collected on a Bio-Rad ''Sting Ray'' instrument equipped with an IR microscope, a step-scanning interferometer, and an infrared detector consisting of an array of 64 ×64 Merucury Cadmum Telluride (MCT) elements (total size ~4×4 mm) imaged to a sample area of ~400×400 μm. Samples were visualized through an optical (visible) microscope monitoring the same area as the IR beam. Samples were positioned as required for data acquisition from the desired region. Interferograms were routinely collected at 8 cm^{-1} spectral resolution, and spectra were generated by Fourier transformation of the 4096 interferograms. Each detector element was sampled 80 times at each stopped position of the moving mirror. Thus the final datasets consist of 4096 IR spectra spanning the frequency range ~900 to 4000 cm^{-1}. The effective range of the MCT elements defines the lower spectral limit. The large datasets (~4 million data points/image) were analyzed with ISYS software supplied by Spectral Dimensions, Incorporated. The software permits a variety of univariate and multivariate manipulations to be performed rapidly on a data cube. In addition, we have on occasion performed principal component analysis (PCA) to enhance image quality.

In the current proof-of-principle study, we have chosen to highlight the spatial variation of a given molecular species within each section, rather than a comparison of concentrations over the entire sample depth. Therefore, the color distribution in each image is ''normalized'' to the mean intensity for that spectral parameter across the 4096 pixels used to construct that image. For many parameters, an equivalent color-to-intensity scale can be used across the entire depth of the skin section. However, if a particular molecular species (endogenous or exogenous) is significantly more concentrated in particular regions of the sample, such image scaling is not feasible without some sections appearing either all red or all blue, and therefore proving no useful information. We believe that a particularly powerful aspect of IR spectroscopic imaging is the ability to directly map molecular species in biological samples, while maintaining sample architecture. The current images emphasis this aspect of the technology.

3 Results

Figure 1 presents typical data from three spectral regions from an 8-μm-thick section cut perpendicular to the skin surface of a sample that had been treated with deuterated propylene glycol (DPG). The isotopic substitution of deuterium atoms into the exogenous molecule provides a useful spectroscopic handle, since the carbon-deuterium stretching modes appear in a spectral region not overlapped by bands from tissue components. Figure 1(a) shows the 1000 to 1800 cm^{-1} region from a single spectrum (of the 4096 collected simultaneously). Several readily identifiable spectral features are observed as labeled on the figure. The intense bands near 1650 and 1550 cm^{-1} arise primarily from the protein amide I (peptide bond C═O stretching vibrations) and amide II (mixed N—H in-plane bending and C—N stretch) vibrations, respectively. The feature near 1720 cm^{-1} arises from ester C═O stretching modes of lipids such as triglycerides and phospholipids, which constitute the vast majority of lipids in the epidermis and dermis. We anticipate that in future studies it may be possible to image the distribution of distinct lipid classes by comparing images of ester, acid, and methylene modes across a biological section. Weaker bands from 1200 to 1500 cm^{-1} are attributable mostly to protein components of the skin and arise from both backbone and amino acid side-chain vibrations. The high frequency region (2700 to 3150 cm^{-1}) shown in Fig. 1(b) (again from a single spectrum) contains C—H stretching vibrations of CH_2 and CH_3 groups. The former occur primarily in lipid constituents of tissue, the latter in protein constituents. Two spectra are shown in Fig. 1(b). The top spectrum arises from a protein-rich region of the tissue section. The weak broadbands, marked in the spectrum at 2870 to 2880 cm^{-1} and 2960 cm^{-1} arise from stretching modes of the methyl group vibrations of the protein (amino acid) side chains. The bottom spectrum arises from a lipid-rich region of the tissue section. Bands near 2850 and 2920 cm^{-1}, strongest in the bottom spectrum, arise primarily from the symmetric and asymmetric CH_2 stretching modes of the lipids.

Figure 1(c) presents an expanded view (averaged from 25 pixels out of the 4096 spectra acquired) of the spectral region 2000 to 2300 cm^{-1}, which reveals the presence of the C—D stretching modes from deuterated propylene glycol ($CD_3CD(OH)CD_2OH$) present in the skin (top spectrum). This assignment is confirmed by comparison with the spectrum of pure DPG shown at the bottom of the figure.

Figure 2 shows the spatial distribution of the protein, lipid, and DPG components in skin in four images generated from spectra acquired from a skin section cut perpendicular to the surface. A visible micrograph of each section is shown in the left-hand panel. The distance from the skin surface (in mi-

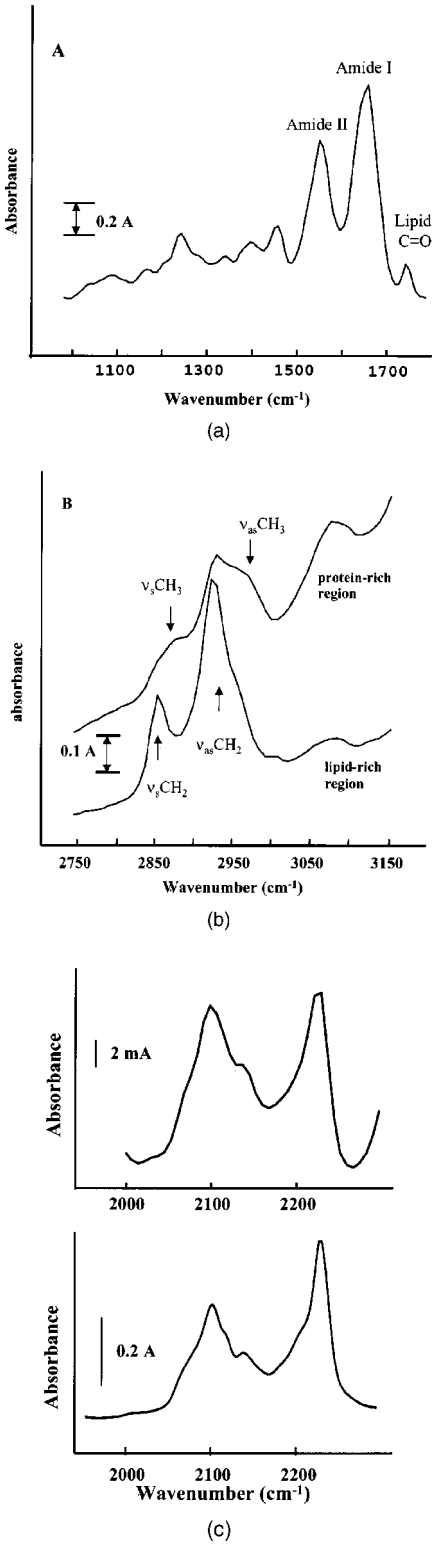

Fig. 1 (a) Typical IR spectrum of the 1000 to 1700 cm^{-1} region of skin. The major spectral features arising from lipid and protein constituents are labeled.[20] (b) Typical C—H stretching regions (2750 to 3150 cm^{-1}) from lipid-rich (bottom trace) and protein-rich (top trace) areas of a skin section. (c) Top trace: The C—D stretching region (2000 to 2300 cm^{-1}) from a skin section containing deuterated propylene glycol. 25 spectra from the set of 4096 have been added to improve the signal-to-noise ratio. Bottom trace: The C—D stretching region (2000 to 2300 cm^{-1}) from a pure sample of deuterated propylene glycol.

crons) is given on the right-hand side of the figure. The color scaling used is red>yellow>green>blue and corresponds to the relative integrated intensity of the given spectral parameter. Relative protein concentration was determined from the intensity of the amide II vibration near 1550 cm^{-1}, while the spatial distribution of polar lipids was estimated from the intensity of the ester C═O stretching mode near 1720 cm^{-1}. The spatial distribution of DPG is depicted in the third vertical panel and was monitored directly from the integrated intensity under the contour formed from the various CD, CD_2, and CD_3 stretching modes depicted in Fig. 1(c).

In Fig. 3, the spatial distribution of DMSO-d_6 is depicted using the same general approach as for the DPG in Fig. 2. A series of visible and IR images, the latter corresponding to the spatial distributions of the protein, DMSO, and lipid components of four images were generated from spectra of a skin section cut perpendicular to the surface layer. The spatial distribution of the protein and lipid constituents were derived from the amide II and C═O intensities, respectively. The DMSO distribution was determined from the peak areas under the CD_3 stretching vibrations. The DMSO distributions as depicted have been subjected to simple image processing methods to improve contrast, as shown in Fig. 4.

An original image of DMSO distribution in a region closest to the skin surface is shown in Fig. 4. This image clearly exhibits substantial noise, traced to the weakness of the original spectral features. This is best demonstrated in the data acquired from the top 50 μm of the image. This area in the field of view does not monitor the skin section, yet shows a pixilated distribution of intensities even though there cannot be any real DMSO intensity present. The absence of substantial numbers of pixels in the histogram of the raw image containing values of zero for the integrated intensity parameter (abscissa) is consistent with this image.

Significant improvement in image quality can be achieved with principal component analysis. This well-known technique yields the eigenvalues of the variance-covariance matrix, and defines components that are responsible for the observed spectral variance. To create an enhanced image, four principal components were retained (which accounted for 99.7% of the variance in the data) and the image was reconstructed with only these four components. The improved image quality is evident, and the histogram of the image shows the expected number of values with a spectral parameter close to zero.

4 Discussion

For elucidation of the mode of action of specific penetration enhancers, as well as for a general understanding of dermal drug delivery mechanisms, it is essential to develop methods that permit direct observation of the spatial distribution of exogenous materials within the skin. The purpose of the current study was to determine the utility of IR imaging microspectroscopy for this purpose. The data clearly demonstrate that IR spectroscopic imaging provides the means to examine the relative concentration of the substance of interest with a spatial resolution approaching the mid-IR diffraction limit. In the current case, the pixel size of 6.3 μm provides the limiting resolution. We have chosen to examine DPG and DMSO-d_6 to develop the IR imaging method for elucidation of penetration pathways in skin.

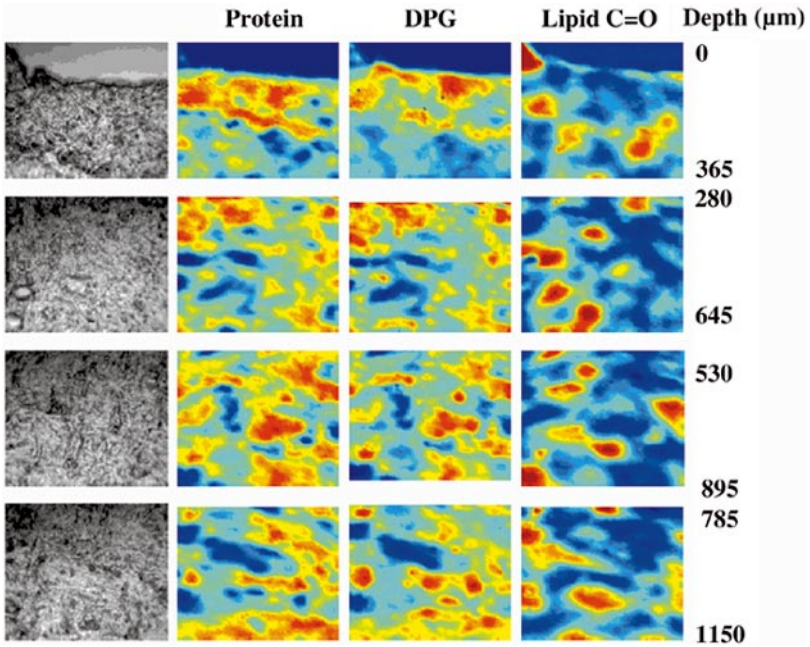

Fig. 2 The spatial distribution of protein, deuterated propylene glycol, and lipid from a section of skin cut perpendicular to the surface. An optical micrograph is included in the left-hand column. Relative protein distribution is estimated from the intensity of the amide II mode; propylene glycol distribution is estimated from the area under all the various C—D stretching vibrations; lipid distribution (phospholipids and triglycerides) is estimated from the ester C═O band intensity. The right-hand scale is the depth from the surface in microns. The vertical images overlap to varying extents as noted. The intensities are color coded as red>yellow>green>blue.

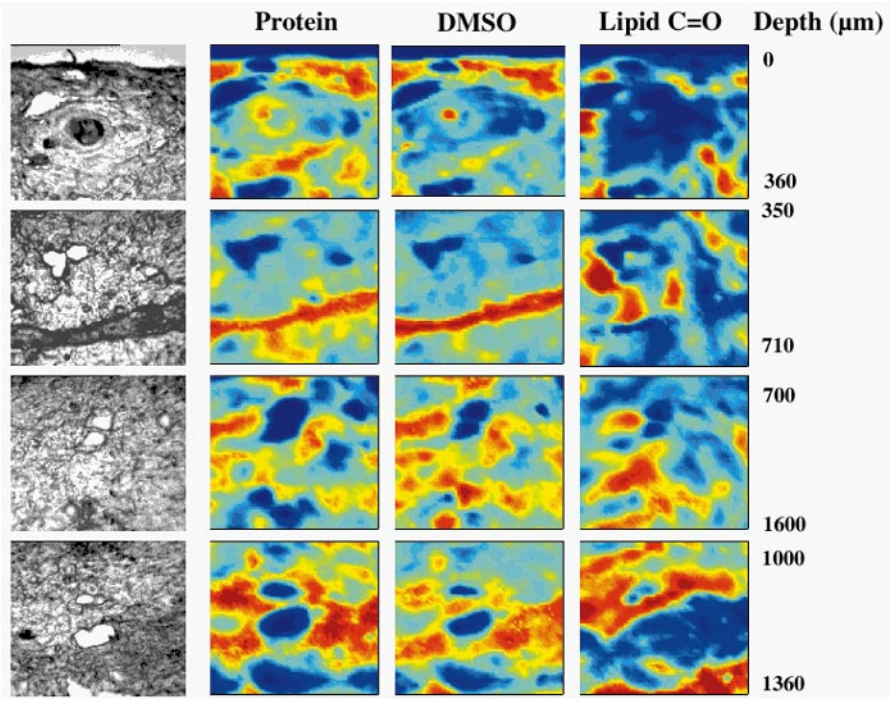

Fig. 3 The spatial distribution of protein, deuterated DMSO, and lipid from a section of skin cut perpendicular to the surface. An optical micrograph of each imaged section is included as the left-hand column. Relative protein distribution is estimated from the intensity of the amide II mode; DMSO distribution is estimated from the area under the CD_3 stretching vibrations (these images are generated after PCA analysis); lipid distribution (phospholipids and triglycerides) is estimated from the C═O band intensity. The right-hand scale is the depth from the surface in microns. The vertical images overlap to varying extents as noted. The intensities are color coded as red>yellow>green>blue.

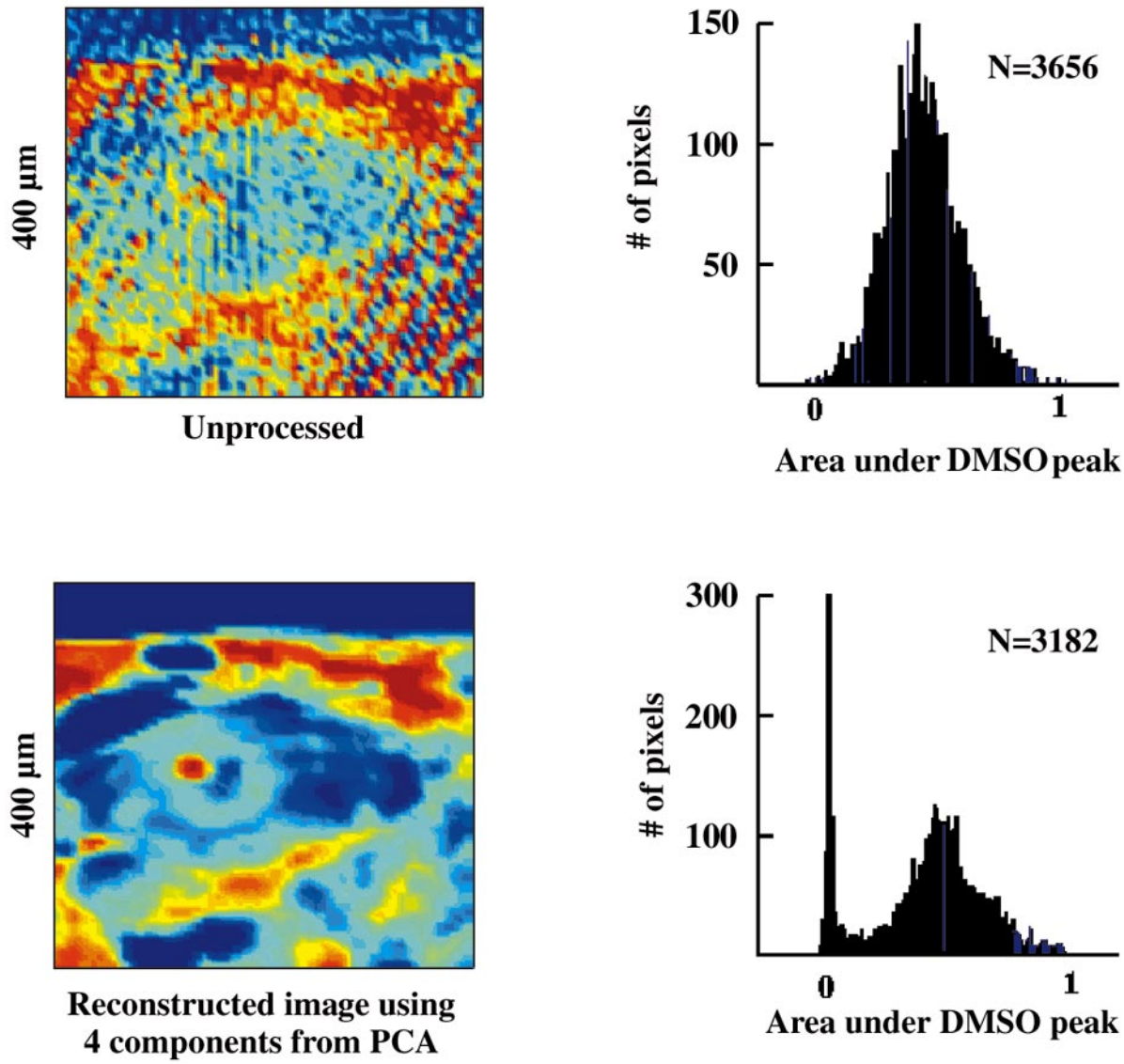

Fig. 4 The effect of image processing on the visualization of deuterated DMSO distribution in a skin section. Top left: Integrated intensity under the CD_3 stretching vibrations. Top right: The histogram of intensity distribution. Bottom left: Integrated intensity under the CD_3 stretching vibrations following application of principal component analysis and reconstruction of the image with the first four principal components. Bottom right: Histogram of intensity distribution in the enhanced image.

As is evident from an examination of Fig. 3, DMSO penetrates skin to a depth of at least 1 mm (under our experimental protocols), and reveals a spatial distribution that is coincident with the protein constituents of the skin. Particularly noteworthy in this regard is the observation in the second row of a dark object at a depth of ~600 μm in the visible image (possibly a hair follicle), which is relatively protein rich and lipid poor. The DMSO is strongly partitioned into this anatomical feature.

Our results substantially extend the earlier work of Higo et al., who used attenuated total-reflectance (ATR-IR) spectroscopy to follow the penetration of 4-cyano-phenol (CP) across human SC.[15] A comparison with tape stripping measurements allowed Higo et al. to validate the equivalent of Beer's Law for CP and, with some limitations, to determine the depth of the CP penetration. Our measurements permit near diffraction-limited spatial resolution of the relative concentration of the exogenous substance, as seen in Figs. 2 and 3 for DPG and DMSO, respectively. Since sections can be prepared either parallel or perpendicular to the skin surface, a reasonably comprehensive spectral mapping of molecular distribution can be obtained in a few images. The penetration of DMSO was mapped (Fig. 3) at depths exceeding 1 mm.

An advantage of the imaging IR approach is that in addition to mapping of exogenous substances in skin, the spatial relationships between the exogenous and endogenous components may be monitored and correlated. It is evident from Figs. 2 and 3 that both DPG and DMSO localize with the protein-rich components of the tissue and suggests that the penetration pathway of these molecules through the epidermis involves protein.

The current proof-of-principle studies clearly demonstrate that IR spectroscopic imaging technology will be a powerful tool in facilitating advances in several areas of dermatological and drug-delivery research. It has been suggested through a combined FT-IR/DSC study that some penetration enhancers, when present during heating processes, enhance an α-helix to β-sheet conversion in the keratin component of porcine SC.[16] PG was found to be quite effective in this process. DSC spectroscopic techniques have also been used to evaluate the effects of DMSO on skin.[17] Several studies have provided evidence that high concentrations of DMSO promote steady-state drug permeation, and delipidation and protein denaturation were suggested as being responsible for the penetration enhancing activity.[18] With current IR imaging technology, it is feasible to examine intact skin sections for the spatial characterization of this process, and to seek relationships between the structural alteration and the relative concentration of the enhancers. Along similar lines, Clancy, Corish, and Corrigan suggested that DMSO caused extensive lipid extraction in addition to protein denaturation.[19] The spatial distribution of these processes should also be readily elucidated with IR imaging. As this technology is further developed, our ability to generate images that map changes in protein secondary structure, or relative ratios of specific endogenous components, will provide a fast and direct method to characterize the molecular changes discussed before. Thus, for example, by mapping the intensity of two distinct components of the protein amide I mode, it will be possible to directly image the relative distribution of protein secondary structure changes across a sample. With these developments, IR spectroscopic imaging technology will move beyond a distribution mapping of components to a mapping of molecular structures and interactions across tissue sections.

References

1. D. Bommannan, R. O. Potts, and R. H. Guy, ''Examination of stratum corneum barrier function in vivo by infrared spectroscopy,'' *J. Invest. Dermatol.* **95**, 403–408 (1990).
2. G. M. Golden, D. B. Guzek, R. R. Harris, J. E. McKie, and R. O. Potts, ''Lipid thermotropic transitions in human stratum corneum,'' *J. Invest. Dermatol.* **86**, 222–259 (1986).
3. D. J. Moore and M. E. Rerek, ''Insights into the molecular organization of lipids in the skin barrier from infrared spectroscopy studies of stratum corneum lipid models,'' *Acta Derm Venereol Suppl. (Stockh)* **208**, 16–22 (2000).
4. R. Mendelsohn and D. J. Moore, ''Infrared determination of conformational order and phase behavior in ceramides and stratum corneum models,'' *Methods Enzymol.* **312**, 228–246 (2000).
5. V. H. W. Mak, R. O. Potts, and R. H. Guy, ''Percutaneous penetration enhancement *in vivo* measured by attenuated total reflectance infrared spectroscopy,'' *Pharm. Res.* **7**, 835–841 (1990).
6. R. O. Potts and M. L. Francoeur, ''Lipid biophysics of water loss through the skin,'' *Proc. Natl. Acad. Sci. U.S.A.* **87**, 3871–3873 (1990).
7. F. Pirot, Y. N. Kalia, A. L. Stinchcomb, G. Keating, A. Bunge, and R. H. Guy, ''Characterization of the permeability barrier of human skin *in vivo*,'' *Proc. Natl. Acad. Sci. U.S.A.* **94**, 1562–1567 (1997).
8. L. M. McIntosh, M. Jackson, H. H. Mantsch, M. F. Stranc, D. Pilavdzic, and A. N. Crowson, ''Infrared spectra of basal cell carcinomas are distinct from non-tumor-bearing skin components,'' *J. Invest. Dermatol.* **112**(6), 951–956 (1999).
9. L. M. McIntosh, R. Summers, M. Jackson, H. H. Mantsch, J. R. Mansfield, M. Howlett, A. N. Crowson, and J. W. Toole, ''Towards non-invasive screening of skin lesions by near-infrared spectroscopy,'' *J. Invest. Dermatol.* **116**(1), 175–181 (2001).
10. R. Mendelsohn, E. P. Paschalis, and A. L. Boskey, ''Infrared spectroscopy, microscopy, and microscopic imaging of mineralizing tissues: spectra-structure correlations from human illiac crest biopsies,'' *J. Biomed. Opt.* **4**, 14–21 (1998).
11. L. H. Kidder, V. F. Kalasinsky, V. F. Luke, I. W. Levin, and E. N. Lewis, ''Visualization of silicone gel in human breast tissue using new infrared imaging spectroscopy,'' *Nat. Med.* **3**, 235–237 (1997).
12. E. N. Lewis, A. M. Gorbach, C. Marcott, and I. W. Levin, ''High fidelity Fourier transform infrared spectroscopic imaging of primate brain tissue,'' *Appl. Spectrosc.* **50**, 263–269 (1996).
13. M. Diem, L. Chiriboga, P. Lasch, and A. Pacifico, ''IR spectra and IR spectral maps of individual normal and cancerous cells,'' *Biopolymers* **267**(4–5), 349–353 (2002).
14. H. Schaefer and T. E. Redelmeier, *Skin Barrier: Principles of Percutaneous Absorption*, Karger, Basel (1996).
15. N. Higo, A. Naik, D. B. Bommannan, R. O. Potts, and R. H. Guy, ''Validation of reflectance infrared spectroscopy as a quantitative method to measure percutaneous absorption in vivo,'' *Pharm. Res.* **10**(10), 1500–1506 (1993).
16. S. Y. Lin, K. J. Duan, and T. C. Lin, ''Microscopic FT-IR/DSC system used to simultaneously investigate the conversion process of protein structure in porcine stratum corneum after pretreatment with skin penetration enhancers,'' *Methods Find Exp. Clin. Pharmacol.* **18**(3), 175–181 (1996).
17. M. Goodman and B. W. Barry, ''Differential scanning calorimetry of human stratum corneum: Effects of penetration enhancers azone and dimethyl sulphoxide,'' *Anal. Proc.* **23**, 397–398 (1986).
18. Z. U. Khan and I. W. Kellaway, ''Differential scanning calorimetry of dimethylsulphoxide-treated human stratum corneum,'' *Int. J. Pharm.* **55**, 129–134 (1989).
19. M. J. Clancy, J. Corish, and O. I. Corrigan, ''A comparison of the effects of electrical current and penetration enhancers on the properties of human skin using spectroscopic (FTIR) and calorimetric (DSC) methods,'' *Int. J. Pharm.* **105**, 47–56 (1994).
20. R. Mendelsohn and H. H. Mantsch, ''Fourier transform infrared studies of lipid-protein interactions,'' in *Progress in Protein-Lipid Interaction*, Vol. 2, A. Watts and J. J. H. M. de Pont, Eds., Elsevier, Amsterdam (1986).